Physics of Fluids ARTICLE scitation.org/journal/phf

On the origin and structure of a stationary circular hydraulic jump

Cite as: Phys. Fluids 31, 072104 (2019); doi: 10.1063/1.5109247
Submitted: 7 May 2019 • Accepted: 7 July 2019 •
Published Online: 25 July 2019

R. Fernandez-Feria,[1,a)] E. Sanmiguel-Rojas,[1] and E. S. Benilov[2]

AFFILIATIONS

[1] Fluid Mechanics, Universidad de Málaga, Dr Ortiz Ramos s/n, 29071 Málaga, Spain
[2] Department of Mathematics and Statistics, University of Limerick, Limerick V94 T9PX, Ireland

[a)] **Electronic mail:** ramon.fernandez@uma.es

ABSTRACT

To elucidate the role played by surface tension on the formation and on the structure of a circular hydraulic jump, the results from three different approaches are compared: the shallow-water (SW) equations without considering surface tension effects, the depth-averaged model (DAM) of the SW equations for a flow with a parabolic velocity profile, and the numerical solutions of the full Navier-Stokes (NS) equations, both considering the effect of surface tension and neglecting it. From the SW equations, the jump can be interpreted as a transition region between two solutions of the DAM, with the jump's location virtually coinciding with a singularity of the DAM's solution, associated with the inner edge of a recirculation region near the bottom. The jump's radius and the flow structure upstream of the jump obtained from the NS simulations practically coincide with the results from the SW equations for any flow rate, liquid properties, and downstream boundary conditions, being practically independent of surface tension. However, the structure of the flow downstream of the jump predicted by the SW equations is quite different from the stationary flow resulting from the NS simulations, which strongly depends on surface tension and on the downstream boundary conditions (radius of the disk). One of the main findings of the present work is that no stationary and axisymmetric circular hydraulic jump is found from the NS simulations above a critical value of the surface tension, which depends on the flow conditions, fluid properties, and downstream conditions.

I. INTRODUCTION

If a thin jet impinges on a disk, the resulting axisymmetric flow is often accompanied by a circular hydraulic jump at a certain radius from the "impingement point." When the flow conditions are such that the jump is stationary, this simple setting provides a rare opportunity to study the structure of hydraulic jumps in general, both experimentally and theoretically. Pioneering papers exploring this problem were those by Tani[1] and Watson,[2] who used the thin-film approximation to describe the flow. Of the huge body of further work, we mention here Refs. 3 and 4, where it was shown that the radius R_j of the stationary jump scales with $Q^{5/8}\nu^{3/8}g^{1/8}$ (Q is the flow rate, ν is the kinematic viscosity, and g the acceleration due to gravity), and Ref. 5, where this scaling was confirmed experimentally.

II. FORMULATION

More precisely, consider an axisymmetric flow from a jet impinging on a horizontal disk and denote the flow's depth scale by H, and the horizontal scale by L. As shown theoretically[3,4] and confirmed experimentally,[5] these are

$$H = \left(\frac{Q\nu}{2\pi g}\right)^{1/4}, \quad L = \left(\frac{Q}{2\pi}\right)^{5/8}\frac{1}{g^{1/8}\nu^{3/8}}. \tag{1}$$

The velocity scale, in turn, is

$$U = \left(\frac{Q\nu}{2\pi}\right)^{1/8} g^{3/8}. \tag{2}$$

Note that scales (1) and (2) correspond to the Froude number and the reduced Reynolds number,

$$Fr = \frac{U^2}{gH}, \quad Re = \frac{UH^2}{\nu L}, \tag{3}$$

being equal to unity. We also introduce the shallow-water (SW) parameter, $\varepsilon = H^2/L^2$, for which (1) implies

$$\varepsilon = \frac{\nu^{5/4}}{g^{1/4}}\left(\frac{2\pi}{Q}\right)^{3/4}.$$

For the recent experiments reported in Refs. 5 and 6, estimates show that ε is quite small. Thus, the shallow-water approximation is applicable to most of their experiments.

Finally, the Bond number, $Bo = \rho g L^2/\sigma$, can be rewritten using (1) in the form

$$Bo = \left(\frac{Q}{2\pi}\right)^{5/4}\frac{\rho}{\sigma}\left(\frac{g}{\nu}\right)^{3/4}, \tag{4}$$

where ρ and σ are the liquid's density and surface tension, respectively. For the recent experiments reported in Refs. 5 and 6 estimates show that Bo is quite large. Thus, surface tension was not generally important, except maybe locally, in regions where the curvature of the free surface happens to be large.

Let the nondimensional vertical coordinate z and the depth h be both scaled by H, the horizontal coordinate r by L, and the radial and vertical components of the velocity, u and v, by U and $\varepsilon^{1/2}U$, respectively. The nondimensional time t is scaled by L/U. Assuming $\varepsilon \ll 1$, one may use the standard shallow-water (SW) equations, which, for a steady radially symmetric flow, take the form

$$\frac{1}{r}\frac{\partial}{\partial r}(ru) + \frac{\partial v}{\partial z} = 0, \tag{5}$$

$$u\frac{\partial u}{\partial r} + v\frac{\partial u}{\partial z} + \frac{\partial h}{\partial r} = \frac{\partial^2 u}{\partial z^2}. \tag{6}$$

Under the shallow-water approximation, the boundary conditions at the free surface are

$$u\frac{\partial h}{\partial r} = v, \quad \frac{\partial u}{\partial z} = 0 \quad \text{at} \quad z = h, \tag{7}$$

and, at the bottom,

$$u = v = 0 \quad \text{at} \quad z = 0. \tag{8}$$

Subject to a suitable condition as $r \to 0$ (which should model the impinging jet), Eqs. (5) and (6) and the boundary conditions (7) and (8) fully determine $u(r, z)$, $v(t, z)$, and $h(r)$. In fact, since this SW model is parameter free, different solutions to the nondimensional problem only arise from different "initial" conditions at different $r = r_0 \ll 1$, where $h = h_0$ and $u = u_0(z)$ should be fixed compatible with the SW model.

In this paper, we shall compare the numerical solution to this SW model with numerical simulations from the full Navier-Stokes (NS) equations for quite different fluids and flow conditions, both without considering the effect of surface tension and including it in the NS simulations.

But first, the physical meaning of the numerical solutions of the SW model, and hence of the main features of the structure of the stationary circular hydraulic jump, can be clarified through a depth-averaged model (DAM) used previously in Refs. 1, 7, and 8 among others. To derive it, integrate Eq. (5) with respect to z from 0 to h, and taking into account the boundary condition (7), write the result in the form

$$r\int_0^h u\,dz = 1, \tag{9}$$

where the constant of integration (nondimensional flux) is set to unity in accordance with our nondimensionalization. Next, integrating Eq. (6) and taking into account condition (7), we obtain

$$\frac{1}{r}\frac{\partial}{\partial r}\left(r\int_0^h u^2 dz\right) + h\frac{\partial h}{\partial r} = -\left(\frac{\partial u}{\partial z}\right)_{z=0}. \tag{10}$$

Following Refs. 1 and 7, we assume the following ansatz:

$$u(r,z) = U(r)\left[\frac{2z}{h(r)} - \frac{z^2}{h^2(r)}\right], \tag{11}$$

where $U(r)$ is the undetermined radial velocity at the free surface. Expression (11) satisfies the boundary conditions (7) and (8) and is close to the solution of Eqs. (5) and (6) in the *lubrication limit*. Outside that, (11) should be treated as a (relatively crude) approximation.

Substitution of (11) into Eq. (9) yields $U(r) = 3/[2rh(r)]$. Inserting the resulting velocity profile into Eq. (10), one can reduce the problem to a single equation for $h(r)$,

$$\frac{dh}{dr} = \frac{3(2h - 5r^2)}{r(5r^2h^3 - 6)}. \tag{12}$$

III. RESULTS AND DISCUSSION

It turns out that, both before and after the shock, the solution of the SW equations follows very closely that of the depth-averaged model. On the shock, the two solutions go separate ways, or rather the numerical solution "switches" from one solution of the DAM to another, as discussed by Kasimov.[7]

Rewrite Eq. (12) in parametric form

$$\frac{dh}{ds} = 3\left(2h - 5r^2\right), \qquad \frac{dr}{ds} = r(5r^2h^3 - 6), \tag{13}$$

where s is the parameter. Equation (13) has a single critical point at $r = (2/5)^{1/2}3^{1/8}$ and $h = 3^{1/4}$, which is a spiral point with roots $\lambda = 9\left(1 \pm i/\sqrt{3}\right)$. Some solutions are plotted in Fig. 1. One can see that they are not single-valued functions $h(r)$ and, thus, cannot represent the problem's global solution.

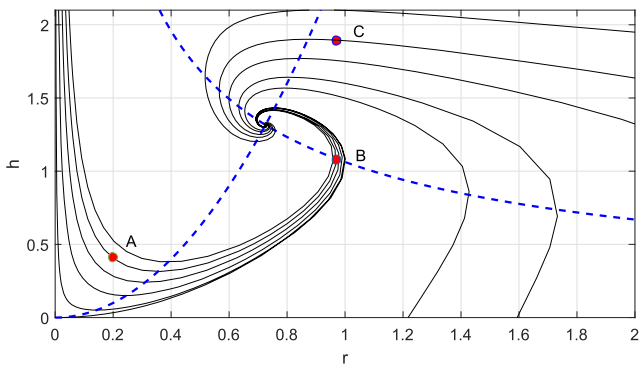

FIG. 1. Some solutions $h(r)$ of Eq. (12) (continuous lines). The dashed lines correspond to the points with $dh/dr = 0$ ($h = 5r^2/2$) and with $dh/dr = \infty$ [$h = (6/5)^{1/3}/r^{2/3}$]; they cross at the critical (spiral) point.

They can still represent the solution in certain regions, i.e., *locally*. For example, the DAM solution originating from the point *A* in Fig. 1 can describe the upstream part of the global flow for a given jet radius and flow rate, while that passing through point *C* may correspond to a downstream boundary condition for a given disk radius (see below). With r increasing, however, the derivative (slope) of the DAM solution grows and eventually becomes infinite at the point *B*. As argued in Refs. 3 and 7, *B* should be a good approximation to the jump's position. Hence, it can be assumed that the "real" solution would veer away from the DAM curve just before reaching *B*, and would jump to, say, point *C*, and continue along the DAM curve passing through this point. Actually, Kasimov[7] performed a more precise computation of the jump's position, within this depth-averaged model, by adjusting the magnitude of the hydraulic jump between the DAM curves passing through the points *A* and *C* for given upstream and downstream boundary conditions, respectively. Notice that Kasimov's approach for the DAM included a bottom topography so that the downstream branch in the DAM could be selected by a downstream boundary condition. The jump location connecting both branches in the DAM was found by this author from continuity of mass and momentum fluxes across the jump. He also considered the effect of surface tension locally to discuss the effect of surface tension on the jump's location within this depth-averaged model.

Here, however, we shall integrate the shallow-water equations to confirm this scenario, where only upstream boundary conditions can be accommodated. The effect of surface tension will be considered later by integrating the full Navier-Stokes equations, where both upstream and downstream boundary conditions can be accommodated.

The system of parabolic equations and boundary conditions (5)–(8) can be solved numerically by using a pseudospectral method of lines,[9] which has proven to be very accurate for this kind of equations even in the presence of small recirculating-flow regions.[10]

Figure 2 shows the numerical solution for $h(r)$ corresponding to the point *A* in Fig. 1, i.e., with $r_0 = 0.2$, $h_0 = 0.4$, and the parabolic velocity profile $u_0(r_0, z)$ given by Eq. (11). As r increases from r_0, the curve $h(r)$ follows closely the corresponding DAM solution [that of Eq. (12)], also shown in Fig. 2. This suggests that the velocity profile in the exact solution remains for a while close to parabolic. Then, the two solutions diverge, and the slope of the exact solution increases suddenly at $r \approx 1$, which is also where the slope of the DAM solution becomes infinite. The jump location also coincides with the radius at which the shear stress at the plate vanishes, marking the beginning of a recirculation region.

Figure 3 is very illustrative of what happens physically at the jump. It shows the three terms of the depth-averaged momentum Eq. (10), but computed with the exact numerical solution of the shallow-water equations for this case. Upstream of the jump the radial momentum flux, $m \equiv \frac{1}{r}\frac{\partial}{\partial r}\left(r\int_0^h u^2 dz\right)$ almost balances the shear stress at the wall $-\tau_f$, the gravitational term $-hh'$ (the prime denotes derivative with respect to r) being almost negligible in comparison with the other two terms. Close to $r = 1$, the shear stress drops suddenly, becoming negative ($-\tau_f$ plotted in the figure becomes positive), but small in magnitude. To compensate this, the gravity term hh' grows abruptly to balance the momentum flux so that a "jump" in h is generated [$h(r)$ is also shown in Fig. 3]. While $-\tau_f$ is negative and small in the recirculating flow region, the momentum flux m is balanced just by gravity (by $-hh'$). After that, inertia becomes negligible ($m \ll 1$), and there exists an almost exact balance between the shear stress at the wall and gravity forces associated with the radial gradient of h. That is to say, downstream of the jump, just after the small region with recirculation, the flow reaches a *lubrication* limit so that the velocity profile is practically parabolic. This is the reason why the curve $h(r)$ fits so well to a solution of Eq. (12) after the jump in Fig. 2. This situation remains valid until h decreases abruptly to zero far downstream (at $r \simeq 3.5$ in the present case), where $|h'|$ becomes very large and the present shallow-water equations are no longer valid (nor, of course, the lubrication approximation).

The solution just described is found for many other starting values of r_0 and h_0, which physically correspond to different values of the jet's radius for a given flow rate since the impinging jet obviously does not satisfy the shallow-water approximation.

Next, we explore the effect of surface tension by solving numerically the full NS equations for different fluids, flow rates, jet diameters, and disk radii. The unsteady numerical simulations were performed in the laminar regime with the computational fluid

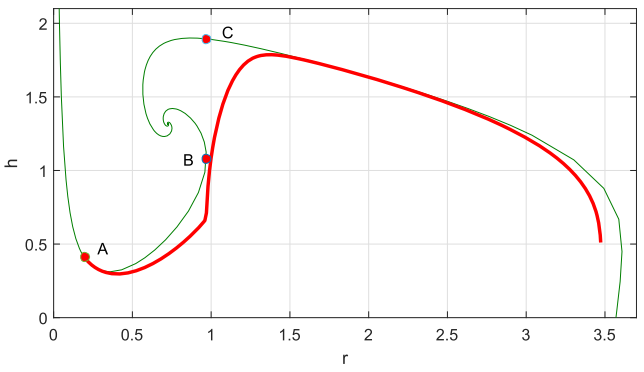

FIG. 2. Solution $h(r)$ of Eqs. (5)–(8), originating from the point *A* in Fig. 1 (thick line). The thin line corresponds to the solutions of Eq. (12).

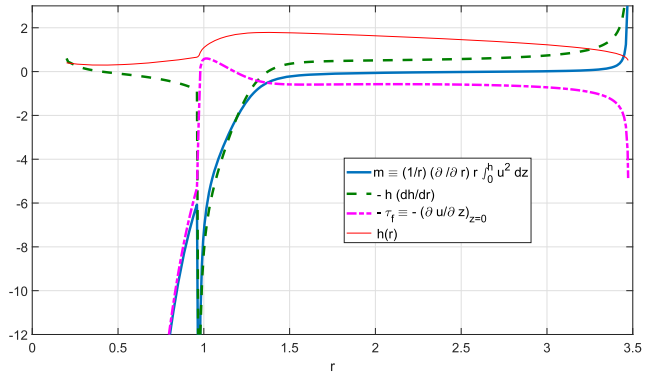

FIG. 3. Radial evolution of the three terms of Eq. (10), as indicated in the legend, for the case considered in Fig. 2. The corresponding $h(r)$ is also plotted with a thinner line.

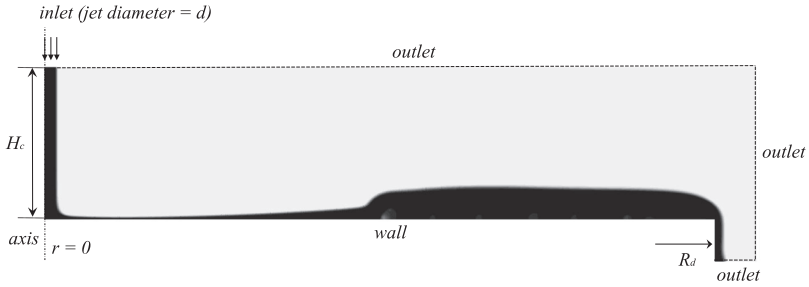

FIG. 4. Computational domain and boundary conditions.

dynamics software ANSYS-Fluent v18.2, using the Volume of Fluid (VoF) method,[11] which has been widely validate with experimental data for unsteady, free surface flows.[12–14] Figure 4 shows the axisymmetric computational domain and the appropriate boundary conditions imposed to get the results under some reported experimental conditions.[6,15] At the inlet, we imposed a jet of uniform velocity profile for the liquid phase, while no-slip conditions were imposed at the solid wall. Outflow conditions were considered at the outlet of the rectangular computational domain. The simulations were carried out with a time step $\Delta t \approx O(10^{-6}$ s) ensuring a Courant number below 0.25. A structured mesh of approximately 10^5 quad elements was chosen after performing an independence grid study. The simulations were calculated in parallel computing with 16 processors intel E5-2670 at 2.6 GHz, 64 GB of RAM memory, and InfiniBand interconnection of 54 Gbits per second. The computations were performed in the Picasso Supercomputer at the University of Málaga, a node of the Spanish Supercomputing Network. The computing time for each simulation was around seven days to simulate 6 physical seconds.

In Fig. 5, we compare the results of the jump radius from our numerical simulations with the values found experimentally in Ref. 6 for a mixture of water and glycerol WG30/70 (70 w/w % of glycerol, density $\rho = 1160$ kg m^{-3}, kinematic viscosity $\nu = 20.7 \times 10^{-6}$ m^2/s, and surface tension $\sigma = 0.067$ N/m, all at 19 °C) with a jet diameter $d = 3$ mm and increasing flow rates. Note that the numerical values fall into the error regions of the experimental data.

Figure 6 shows the numerical results for the dimensional liquid height once a stationary state has been reached for two radius of the target disk, $R_d = 80$ mm and 120 mm, both taking into account the surface tension and without considering it (i.e., by setting $\sigma = 0$ in the numerical simulation). In addition to the water-glycerol mixture WG30/70 described above, with $Q = 5$ l/min and $d = 3$ mm, we also consider another water-glycerol mixture with much higher viscosity (WG10/90, with $\rho = 1240$ kg m^{-3}, $\nu = 99.3 \times 10^{-6}$ m^2/s, $\sigma = 0.065$ N/m, all at 19 °C), for $Q = 10$ l/min, and the same jet diameter and disk radii. Finally, we also consider pure water ($\rho = 1000$ kg m^{-3}, $\nu = 1.00 \times 10^{-6}$ m^2/s, $\sigma = 0.072$ N/m) with a much smaller flow rate ($Q = 0.6$ l/min) and double jet diameter ($d = 6$ mm), the same two disk radii, but now only without taking into account surface tension ($\sigma = 0$), because no steady flow is reached for water when its actual surface tension is used (all the corresponding temporal evolutions are recorded in videos 1–12 of the supplementary material, including those for water with $\sigma = 0.072$ N/m). In all cases, the jet Reynolds number is low enough to ensure laminar flow: $Re_{jet} = 4Q/(\pi d\nu) = 1709$, 712, and 2121, respectively.

Figure 7 shows the nondimensional stationary liquid heights $h(r)$, obtained by scaling the profiles in Fig. 6 with the corresponding vertical (H) and radial (L) lengths, together with the SW solutions obtained by solving (5)–(8) starting from $r_0 = 0.15$ and $h_0 = 0.127$ when the jet diameter is $d = 3$ mm (WG30/70 and WG10/90) and from $r_0 = 0.15$ and $h_0 = 0.89$ for $d = 6$ mm (water). It is remarkable that, despite the great diversity in the profiles observed in Fig. 6, all of them collapse upstream of the hydraulic jump and coincide with

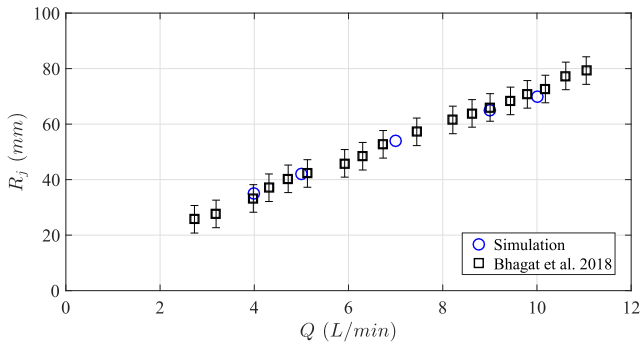

FIG. 5. Jump radius R_j vs flow rate Q from our numerical results (circles) compared to the experimental results by Bhagat *et al.*[6] (squares) for a water-glycerol mixture WG30/70.

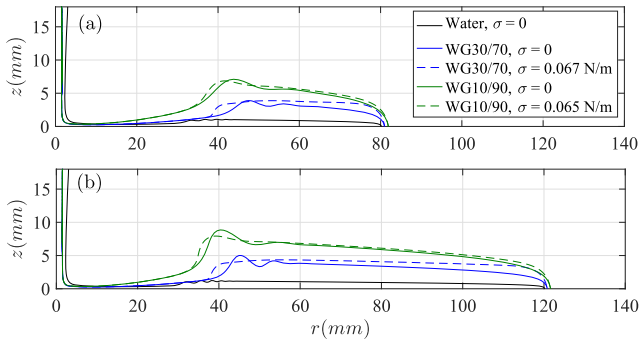

FIG. 6. Stationary liquid film profiles (dimensional) obtained numerically from the NS equations for three liquids and different flow rates (see the main text), for jets of different diameters impinging on two disks with different radius, 80 mm (a) and 120 mm (b), with and without considering the effect of surface tension (except for water, which is only plotted for $\sigma = 0$ because no stationary flow is reached when using its actual surface tension $\sigma = 0.072$ N/m). The temporal evolution of the different flows is given in videos 1–10 of the supplementary material.

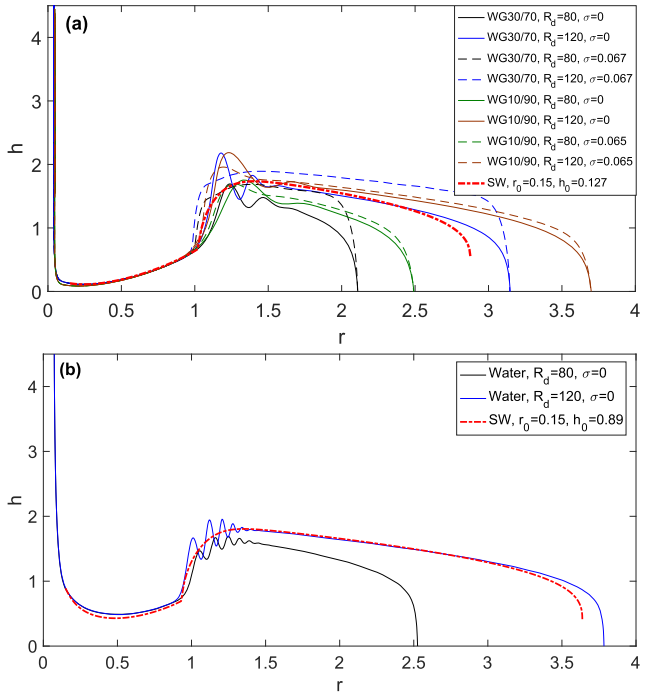

FIG. 7. Nondimensional profiles $h(r)$ corresponding to the numerical results plotted in Fig. 6. Also included are the SW solutions of (5)–(8) starting from $r_0 = 0.15$, $h_0 = 0.127$ (a), and $r_0 = 0.15$, $h_0 = 0.89$ (b).

the solution of the SW model, which predicts quite accurately the hydraulic jump as $r = r_j \approx 1$. This shows that, if the hydraulic jump is stationary, its radius is practically independent not only of the downstream boundary conditions (i.e., of the radius of the disk), but also of the surface tension. However, the shape of the crest following the jump strongly depends on surface tension so that the nondimensional downstream liquid height profile for a given disk radius is quite different whether surface tension is considered or not.

Surface tension is also essential for the stability of the axisymmetric hydraulic jump. In fact, as mentioned above, in the case of water and the flow conditions considered in Fig. 6, the numerical simulations do not reach a steady flow when its actual surface tension in air is used. We have repeated the numerical simulations for increasing values of σ, starting from $\sigma = 0$ (only for a disk radius $R_d = 80$ mm), and found that no steady flow is reached above a critical value σ^* which is in the range $0.025\sigma_a < \sigma^* < 0.05\sigma_a$, where $\sigma_a = 0.072$ N/m is the actual surface tension of water. These numerical experiments have been repeated for the water-glycerol mixture WG30/70, starting from its actual surface tension in air (now $\sigma_a = 0.067$ N/m; remember that the flow with $\sigma = \sigma_a$ become stationary for both R_d considered in Fig. 6, see videos 1–4 in the supplementary material). The minimum surface tension above which the flow is no longer stationary is found to lay now between $1.5\sigma_a$ and $1.75\sigma_a$. These critical values of the surface tension for these two liquids with a disk radius $R_d = 80$ mm are recorded in Table I together with the corresponding Weber number [$We = \rho U^2 H/\sigma$, with H and U given by (1) and (2), respectively] and Bond number (4). It seems

TABLE I. Critical surface tension above which no stationary solution is reached, and the corresponding Weber and Bond numbers, for two of the flows considered in Fig. 6(a). See videos 11 and 12 in the supplementary material.

Liquid	r_d	σ^*/σ_a	We	Bo
Water	2.52	0.025—0.05	2.20 — 1.10	5505 — 2753
WG30/70	2.08	1.5—1.75	0.60 — 0.51	166.9 — 143.0

that the hydraulic jump does not remain stationary below a critical Weber number that depends on the nondimensional disk size, $r_d = R_d/L$, which is also given in Table I. The instability seems to be caused by capillary waves propagating upstream from the downstream boundary condition, recalling those associated with elastic jumps on elastic tubes.[16] But their analysis and characterization in terms of the nondimensional disk radius and Weber number lies out of the scope of the present paper.

IV. CONCLUSION

In conclusion, we find that the radius of a stationary and axisymmetric circular hydraulic jump and the flow structure upstream of the jump are well predicted by the shallow water approximation, and do not depend on the surface tension and the conditions downstream of the jump. Thus, the nondimensional location of the jump turns out to be independent of the problem's parameters, in agreement with full numerical simulations validated experimentally. The jump can be interpreted as a transition region between two solutions of the depth-averaged model for a flow with a parabolic velocity profile. The numerical solution of the shallow-water equations show that the jump's location virtually coincides with a singularity of the solution of the DAM, and it is associated with the beginning of a recirculation region near the bottom. At this recirculation region, the numerical solution of the "parabolic" SW model becomes locally imprecise so that it arbitrarily selects one of the downstream solutions of the DAM. Precise numerical simulations from the full NS equations show that the flow downstream of the jump depends strongly on surface tension and on the downstream boundary conditions. In fact, we find that when surface tension is above (Weber number is below) a critical value, which depends on the (nondimensional) disk radius, a stationary circular hydraulic jump no longer exists.

SUPPLEMENTARY MATERIAL

See supplementary material for the videos corresponding to Fig. 6 and Table I.

ACKNOWLEDGMENTS

This work was partially financed by the mobility grant *Salvador de Madariaga* Grant No. PRX18/050, from the Spanish *Ministerio de Ciencia, Innovación y Universidades.*

REFERENCES

[1] I. Tani, "Water jump in the boundary layer," J. Phys. Soc. Jpn. **4**, 212–215 (1949).
[2] E. J. Watson, "The radial spread of a liquid jet over a horizontal plane," J. Fluid Mech. **20**, 481–499 (1964).

[3]T. Bohr, P. Dimon, and V. Putkaradze, "Shallow-water approach to the circular hydraulic jump," J. Fluid Mech. **254**, 635–648 (1993).
[4]T. Bohr, V. Putkaradze, and S. Watanabe, "Averaging theory for the structure of hydraulic jumps and separation in laminar free-surface flows," Phys. Rev. Lett. **79**, 1038–1041 (1997).
[5]A. Duchesne, L. Lebon, and L. Limat, "Constant Froude number in a circular hydraulic jump and its implication on the jump radius selection," Europhys. Lett. **107**, 54002 (2014).
[6]R. K. Bhagat, N. K. Jah, P. F. Linden, and D. Ian Wilson, "On the origin of the circular hydraulic jump in a thin liquid film," J. Fluid Mech. **851**, R5 (2018).
[7]A. R. Kasimov, "A stationary circular hydraulic jump, the limits of its existence and its gasdynamic analogue," J. Fluid Mech. **601**, 189–198 (2008).
[8]Y. Wang and R. E. Khayat, "The role of gravity in the prediction of the circular hydraulic jump radius for high-viscosity liquids," J. Fluid Mech. **862**, 128–161 (2019).
[9]R. Fernandez-Feria and J. Ortega-Casanova, "A pseudospectral based method of lines for solving integro-differential boundary-layer equations," Appl. Math. Comput. **242**, 388–396 (2014).
[10]R. Fernandez-Feria, C. del Pino, and A. Fernandez-Gutierrez, "Separation in the mixed convection boundary-layer radial flow over a constant temperature horizontal plate," Phys. Fluids **26**, 103603 (2014).
[11]C. W. Hirt and B. D. Nichols, "Volume of fluid (VOF) method for the dynamics of free boundaries," J. Comput. Phys. **39**, 201–225 (1981).
[12]R. Bolaños-Jiménez, A. Sevilla, C. Gutiérrez-Montes, E. Sanmiguel-Rojas, and C. Martínez-Bazán, "Bubbling and jetting regimes in planar coflowing air–water sheets," J. Fluid Mech. **682**, 519–542 (2011).
[13]L. A. Teran, S. A. Rodríguez, S. Laín, and S. Jung, "Interaction of particles with a cavitation bubble near a solid wall," Phys. Fluids **30**, 123304 (2018).
[14]V. C. Todkari and R. P. Kate, "Numerical and experimental investigations on a circular hydraulic jump due to normal impinging free liquid jet on a flat horizontal target plate," Fluid Dyn. Res. **51**, 025508 (2019).
[15]G. J. Jameson, C. E. Jenkins, E. C. Button, and J. E. Sader, "Water bells formed on the underside of a horizontal plate. Part 1. Experimental investigation," J. Fluid Mech. **649**, 19–43 (2010).
[16]S. J. Cowley, "On the wavetrains associated with elastic jumps on fluid-filled elastic tubes," Q. J. Mech. Appl. Math. **36**, 289–312 (1983).